Phase Equilibria in the Fe-Al-Nb(-B) System at 700 °C

A. Gedsun[1] · F. Stein[1] · M. Palm[1]

Abstract Within a composition range that is of interest for future alloy developments and at a possible application temperature of 700 °C, phase equilibria between Fe_3Al and the $Nb(Fe,Al)_2$ Laves phase have been determined. It was found that the solid solubility for Nb in Fe-Al increases by five times, when the Al content increases from about 25 to 35 at.% Al. Besides, the compositions of the co-existing phases, their lattice constants, Curie temperatures, transition temperatures and the solidus and liquidus temperatures of the Fe-Al-Nb alloys, some additionally doped with boron, have been determined.

Keywords intermetallics · phase equilibria · solubility limit

1 Introduction

Due to their outstanding corrosion and wear resistance and comparably low density, iron aluminide-based alloys are suitable materials for structural applications at high temperatures.[1–3] However, for a wider usage ductility at lower temperatures should be improved and, more important, strength above 500 °C has to be increased.[4] Through alloying, the mechanical properties of iron aluminide-based alloys can be further enhanced by solid-solution hardening or strengthening by precipitates like borides, carbides, or other intermetallic phases.[5,6]

For the alloy development of iron aluminide-based materials, the Fe-Al-Nb system is of great importance. Strengthening through solid-solution hardening is limited within this system by the limited solid solubility of Nb in Fe-Al[7] (the term "Fe-Al" is used when the ordering in the body centred cubic Fe-based matrix is not explicitly considered, which could be ordered $D0_3$ in Fe_3Al, B2 in FeAl or disordered A2 for (αFe, Al) solid solution for the same composition depending on temperature). However, homogeneously distributed precipitates of the C14-ordered Laves phase $Nb(Fe,Al)_2$ in the Fe-Al matrix lead to higher yield strength, creep resistance and hardness.[2,8–12] The strength can also be improved by metastable $L2_1$-ordered Heusler phase (Fe_2AlNb) precipitates.[13,14] Through controlled microstructural engineering, the sought mechanical properties can be achieved in these alloys. Therefore, a deeper understanding of the phase equilibria in the iron corner of the Fe-Al-Nb system is essential, specifically at the envisaged application temperatures of around 700 °C.

A recent critical assessment[7] and thermodynamic descriptions[15–17] of the Fe-Al-Nb system are available. The critical assessment[7] contains evaluations of the isothermal sections at 800 °C,[15,18,19] 1000 °C,[15,16,19–21] 1150 °C,[15,16,19,21] 1170 °C,[22] 1300 °C and 1450 °C,[15,16,21] a liquidus projection,[15,16,21] a reaction scheme and crystallographic data for the relevant phases. An isothermal section at 1400 °C has been established on the basis of additional experiments in the Nb-rich part and CALPHAD modelling.[17] Metastable isotherms for 627, 827 and 1027 °C, showing the homogeneity ranges of the Heusler phase ($L2_1$), FeAl (B2) and (αFe, Al) (A2) were calculated using the cluster variation method (CVM).[23]

Phase equilibria in the Fe corner of the Fe-Al-Nb system within the investigated temperature range from 800 to 1450 °C are formed between (αFe, Al) or FeAl and the

✉ A. Gedsun
a.gedsun@mpie.de

1 Max-Planck-Institut Für Eisenforschung GmbH, Max-Planck-Str. 1, Düsseldorf, Germany

Laves phase Nb(Fe,Al)$_2$, which shows a solubility of up to 50 at.% Al.[7,19] Like in the binary Fe-Nb system, the Laves phase also shows a considerable variation in the Nb content within the ternary system, which varies between about 27 to 35 at.% Nb.[19,21] The Nb solubility in Fe-Al is limited and increases with increasing Al content. In disordered (αFe, Al) below 20 at.% Al, the solubility of Nb slightly increases with increasing temperature from about 0.2 at.% Nb at 800 °C to about 1 at.% at 1150 °C and 1300 °C.[22] For a given temperature the Nb content increases when disordered (αFe, Al) becomes ordered FeAl with increasing Al content. However, in FeAl the Nb solubility decreases when the temperature is raised from 800 to 1150 °C.[19]

The effect of Nb addition on the transition temperature from D0$_3$-ordered Fe$_3$Al to B2-ordered FeAl and from FeAl to disordered A2 (αFe, Al) was studied before.[21,24,25] It was found that both transition temperatures increase with increasing Nb content, which is also in accordance with thermodynamic calculations.[24,26]

While the lattice parameter of Fe-Al(+ Nb) shows a complex dependence on the Al content and is affected by the temperature from which the alloy has been quenched,[19,27–30] the lattice parameters of the Laves phase Nb(Fe,Al)$_2$ increase with increasing Al content and are not influenced by the temperature from which the phase has been quenched.[19]

The present investigation aims to elucidate the phase equilibria in the Fe-Al-Nb system at 700 °C, which is a possible application temperature for iron aluminide-based alloys, e.g. in stationary turbines. Specific emphasis lies on the determination of the solid solubility of Nb in Fe-Al with Al content of about 25 to 35 at.%, i.e. for Al contents where a good balance between ductility, strength, and corrosion resistance is obtained,[3] and where Fe-Al is in equilibrium with the Laves phase. These data are substantial for prospective alloy developments for adjusting the volume fraction of the Laves phase, which has a crucial effect on the mechanical properties of these alloys.[31] A second aim is the determination of the transition temperatures of Fe-Al, because specifically the transition from face-centred cubic Fe$_3$Al to simple cubic FeAl leads to a substantial loss in strength.[6]

The difficulty of determining the phase equilibria at 700 °C in this system is not only the sluggish diffusion of Nb[32–34] at this temperature, but also the formation of the metastable Heusler phase.[13,14] When the Fe-Al matrix becomes supersaturated with Nb on cooling, the Heusler phase precipitates instead of the stable Laves phase. The same has been observed in the Fe-Al-Ta system, where coherent precipitates of the Heusler phase form within the Fe-Al matrix on cooling and where the Laves phase forms only after prolonged annealing, preferably on grain boundaries and at other nucleation sites.[33,35] In the Fe-Al-Ta system, the Heusler phase is still observed after 10,000 h annealing at 700 °C together with the Laves phase. However, by doping with boron or inducing a high dislocation density by thermomechanical processing, formation of the stable Laves phase can be accelerated.[10,35] Therefore, some of the alloys used in this investigation were doped with boron and the doping effect on phase equilibria, transition temperatures, lattice parameters and precipitation formation has been studied.

2 Experimental

Eleven Fe-Al-Nb(-B) alloys with Al contents between 25 and 34 at.% and containing 2 to 3 at.% Nb, partially doped with boron (< 100 ppm), were produced by vacuum induction melting from pure Fe (99.9 wt.%), Al (99.9 wt.%), Nb (99.9 wt.%) and B (99.4 wt.%) under argon and cast into copper molds of 20 mm diameter. The actual compositions of all alloys, as determined by wet chemical analysis, are shown in Table 1. The as-cast alloys were heat-treated at 700 °C for 1000 h in air to reach thermodynamic equilibrium of the phases. Because the samples were also used for mechanical testing, they were not quenched, but furnace cooled. In view of the comparatively low annealing temperature and the slow diffusion of Nb, this practice seemed reasonable, and the investigation yielded no indication of any changes of the phase equilibria during cooling. The microstructure of the alloys in the as-cast condition and after heat treatment was inspected by scanning electron microscopy (SEM; Zeiss LEO 1550 VP) on metallographic sections, which were ground and polished up to 0.5 µm with a diamond particle suspension. Additional preparation with an oxide polishing suspension (OPS + H$_2$O$_2$) for a few seconds was used in a few cases to avoid mechanical etching of the Laves phase on the grain boundaries.

The chemical compositions of the phases were established by wavelength-dispersive electron probe microanalysis (EPMA; Jeol JXA-8100). Quantitative analysis was performed at 15 kV and 20 nA using pure elements as standards. At least 15 to 20 measurements for each phase and at different positions on the specimen were performed.

Phases were characterized by x-ray diffraction (XRD; Bruker D8 Advance A25) on metallographic sections by scanning the 2θ-range from 20° to 125° using Co-Kα_1 radiation (λ = 0.178897 nm). Lattice parameters of the phases were calculated using the TOPAS software package.[36] Volume factions of the coexisting phases were calculated from alloy and phase compositions and the lattice constants using the lever rule.

Table 1 Actual alloy compositions as determined through wet-chemical analysis and compositions and volume fractions of the coexisting phases after heat treatment 700 °C/1000 h as determined by EPMA and XRD. Data are partially taken from previous research[37]

Alloy	Fe₃Al matrix				Laves phase			
Analysed composition, at.%	at.% Fe	at.% Al	at.% Nb	Volume fraction	at.% Fe	at.% Al	at.% Nb	Volume fraction
Fe-24.4Al-2Nb-0.03B[37]	74.4 ± 0.7	25.2 ± 0.6	0.4 ± 0.1	0.93	59.7 ± 1.3	17.0 ± 0.6	23.3 ± 1.7	0.07
Fe-25.7Al-2Nb	73.8 ± 0.2	25.6 ± 0.2	0.6 ± 0.1	0.93	60.2 ± 1.4	17.3 ± 0.5	22.5 ± 1.8	0.07
Fe-25.7Al-2Nb-0.01B	73.1 ± 0.4	26.2 ± 0.4	0.7 ± 0.2	0.95	57.9 ± 1.0	17.3 ± 0.9	24.8 ± 0.8	0.05
Fe-27.7Al-2Nb	71.3 ± 0.4	27.8 ± 0.4	0.9 ± 0.1	0.95	57.1 ± 1.0	17.8 ± 0.8	25.1 ± 1.0	0.05
Fe-27.7Al-2Nb-0.01B	70.9 ± 0.2	28.2 ± 0.2	0.9 ± 0.1	0.96	56.4 ± 1.3	18.1 ± 0.6	25.5 ± 1.6	0.04
Fe-27.7Al-3Nb	69.8 ± 0.5	29.2 ± 0.5	1.0 ± 0.1	0.91	55.0 ± 1.4	19.5 ± 1.5	25.5 ± 1.6	0.09
Fe-27.7Al-3Nb-0.01B	69.6 ± 0.5	29.4 ± 0.4	1.0 ± 0.1	0.91	54.6 ± 1.4	20.0 ± 1.4	25.4 ± 0.9	0.09
Fe-31.9Al-3Nb[37]	66.2 ± 0.2	32.0 ± 0.3	1.8 ± 0.2	0.95	52.5 ± 1.0	21.9 ± 1.2	25.6 ± 0.6	0.05
Fe-31Al-3Nb-0.06B[37]	65.6 ± 0.3	32.5 ± 0.3	1.9 ± 0.2	0.94	52.7 ± 1.0	22.1 ± 0.6	25.2 ± 0.7	0.06
Fe-33.6Al-3Nb[37]	64.2 ± 0.6	33.6 ± 0.4	2.2 ± 0.2	0.96	52.0 ± 0.9	23.1 ± 0.6	24.9 ± 0.7	0.04
Fe-33.6Al-3Nb-0.03B[37]	63.1 ± 0.4	34.4 ± 0.1	2.5 ± 0.3	0.97	51.5 ± 1.5	23.5 ± 0.6	25.0 ± 1.8	0.03

For the determination of the transition temperatures, differential thermal analysis (DTA; NETZSCH STA 449 F3 Jupiter) was carried out up to 1200 °C under Ar with heating and cooling rates of 10 or 20 K/min on selected heat-treated samples. The temperatures of the second-order reactions were determined at the maximum of the endothermic peaks. The determination of the solidus and liquidus temperatures was carried out in additional experiments, whereas-cast alloys were heated up to 1550 °C with heating and cooling rates of 10 K/min. The solidus temperature is determined from the onset of the strongest endothermic peak of the heating curve, while the liquidus temperature is the mean value between the peak maximum of the strongest endothermic peak of the heating curve and the onset temperature of the strongest exothermic peak of the cooling curve.

High-temperature XRD (HT-XRD; RIGAKU SmartLab 9 kW) was carried out to allocate transition temperatures determined by DTA to certain phase transformations. Before the first measurement, the samples were annealed *in-situ* at 500 °C for 30 min. Actual measurements were carried out at temperatures approximately 20 °C above and below the transformation temperatures, previously determined by DTA, with a 2θ scan range of 20° to 50° and a scan rate of 0.75°/min. Room temperature measurements were taken before and after the measurements within a 2θ scan range 20° to 100° applying a scan rate of 1°/min.

3 Results and Discussion

3.1 Phase Characterizations and Microstructures

Phases were identified by XRD and their compositions were established by EPMA. The chemical compositions of the alloys as determined by wet-chemical analysis as well as the compositions and the volume fractions of the coexisting phases after heat treatment are given in Table 1. The boron content in the boron-doped alloys was in the range of the measurement uncertainty of the EPMA and is therefore not further considered.

The microstructural development at 700 °C in dependence on annealing time was investigated and reported before.[37] After 1 h at 700 °C, the metastable Heusler phase formed coherent precipitates in Fe-24.4Al-2Nb-0.03B, but not in alloys with higher Al content, which completely dissolved after 100 h.[37] Figure 1 shows a typical microstructure after 1000 h annealing at 700 °C for two of the investigated alloys with different compositions. Laves phase precipitates are lining the grain boundaries and are distributed in the grains of the Fe-Al matrix in all investigated alloys.

3.2 Partial Isothermal Section at 700 °C

The partial isothermal section of the Fe-rich corner of the ternary Fe-Al-Nb system at 700 °C as established from the EPMA measurements is shown in Fig. 2. The homogeneity ranges of (αFe, Al) solid solution and FeAl in the binary system at 700 °C are taken from,[38] the homogeneity range of the binary Laves phase NbFe₂ is taken from[16] and the solid solubility of Nb in Fe at 700 °C from.[39] All tie-lines, connecting the two coexisting phases, run through the
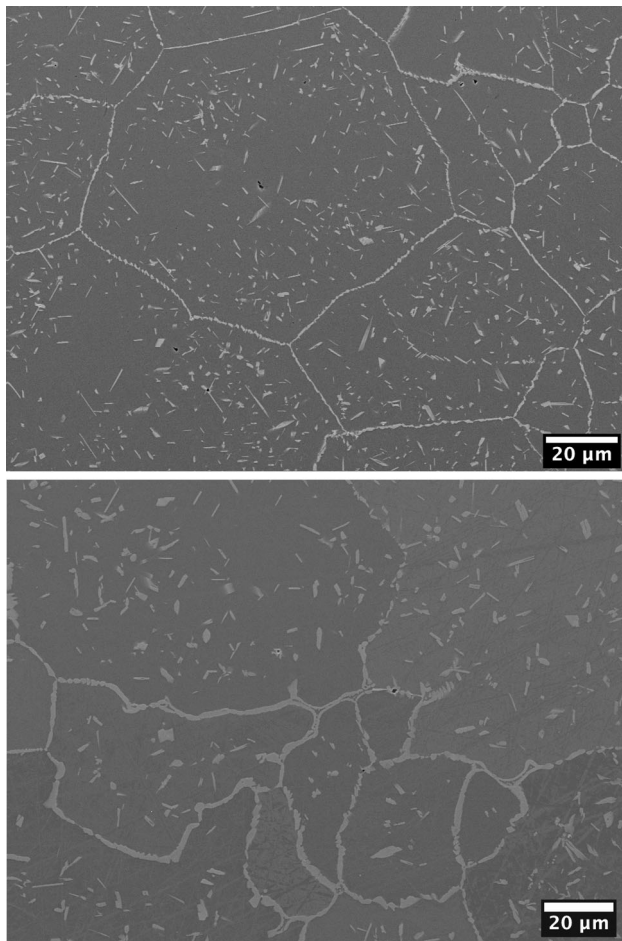
Fig. 1 Back-scattered electron (BSE) micrographs of (a) Fe-25.7Al-2Nb and (b) Fe-27.7Al-3Nb after 700 °C /1000 h, showing the Fe-Al matrix (grey) and the Laves phase (bright phase)
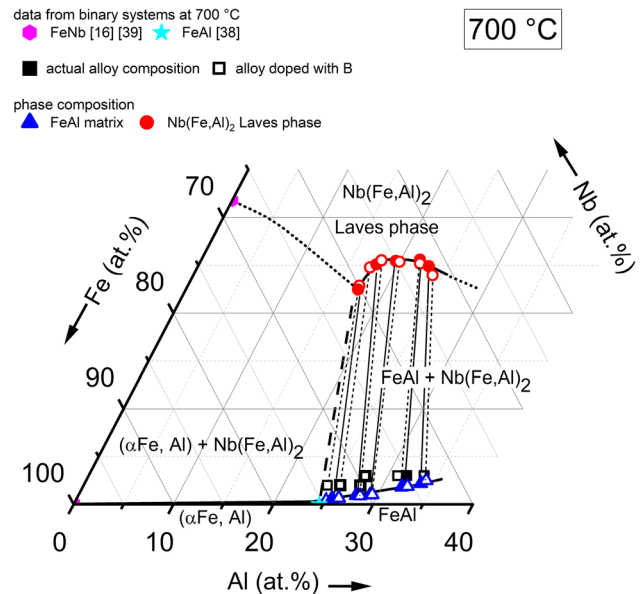

Fig. 2 Partial Isothermal section of the Fe-Al-Nb system at 700 °C. Circles (red) mark the chemical compositions of the $Nb(Fe,Al)_2$ Laves phase and triangles (blue) of the FeAl matrix. The actual compositions of the alloys are represented by square-shaped (black) symbols. Open symbols, connected with dashed tie-lines, indicate that this alloy was doped with boron. The composition of the Laves phase and homogeneity ranges of the (αFe, Al) and FeAl in the binary systems are taken from[16,39]and[38] respectively (Color figure online)

actual compositions of the alloys and their slope changes continuously, indicating that equilibrium has been attained in all samples and that there is no conflict between individual measurements. In Fig. 2, open symbols, connected with dashed tie-lines, indicate that this alloy was doped with boron. Comparison with the results of the boron-free alloys shows that the doping with boron apparently did not influence the phase equilibria.

All alloys are located within the two-phase field FeAl + $Nb(Fe,Al)_2$. The minimum Nb content in the $Nb(Fe,Al)_2$ Laves phase decreases with increasing Al content as long as $Nb(Fe,Al)_2$ is in equilibrium with (αFe, Al), as indicated with the dotted line in Fig. 2. The isothermal sections at higher temperatures do not show such an initial decrease of the Nb content in $Nb(Fe,Al)_2$ with increasing Al content. However, also in the Fe-Al-X (X = Ti, Zr) systems, where a $X(Fe,Al)_2$ Laves phase is in equilibrium with (αFe, Al), the content of X decreases in $X(Fe,Al)_2$ with increasing Al content.[40] In equilibrium with FeAl, the Nb content in $Nb(Fe,Al)_2$ increases with

increasing Al content (solid line in Fig. 2). Whether the Nb content in $Nb(Fe,Al)_2$ then becomes constant at even higher Al contents or decreases again, as the current data indicate, cannot be decided from the current experiments. In the isothermal section at 800 °C, a slight increase of the Nb content in $Nb(Fe,Al)_2$ is observed with increasing Al content when in equilibrium with FeAl.[7]

The discontinuous change of the slope in the $Nb(Fe,Al)_2$ phase boundary in the present isothermal section at 700 °C can be explained with the existence of a three-phase equilibrium (αFe, Al) + FeAl + $Nb(Fe,Al)_2$. Though this three-phase equilibrium has not been directly determined in this study, it should be very close to the tie-lines of the most Al-lean alloy in Fig. 2. Whether the transition from (αFe, Al) to FeAl is still a second order transition, like in the binary system, or if it becomes a first order transition, cannot be decided from the current experimental evidence. In Fig. 2 it is shown by a dashed line, indicating a second order transition, in agreement with the representations of isothermal sections at higher temperatures, where also a second order transition is assumed.[7,19]

3.3 Niobium Solid Solubility in (αFe, Al) and FeAl

Figure 3 shows the Nb solid solubility in the Fe-Al matrix in dependence on the Al content at 700 °C and in

comparison to higher temperatures.[22] At 700 °C, the solid solubility increases with increasing Al content from 0.5 to 1 at.% Nb for 25 to 30 at.% Al. Above 30 at.% Al, this increase becomes stronger and the solubility reaches a value of 2.5 at.% Nb. It is noted that the data are in perfect agreement with those determined in a preliminary study on boron-doped alloys.[41] An influence of the boron doping on the Nb solubility was not observed. The Nb solid solubility increases with the Al content at each temperature, and at all temperatures a pronounced increase in the slope is observed. At least in the temperature range 700 to 1000 °C this increase is in the composition range where the transition from disordered (αFe, Al) to ordered FeAl, indicated by straight vertical lines in Fig. 3, takes place. Within (αFe, Al), the solid solubility for Nb is quite limited, does not markedly change in dependence on the Al content, and increases with increasing temperature. In FeAl, the solid solubility for Nb at all temperatures is markedly higher than in (αFe, Al) and increases significantly with increasing Al content. The increase is the higher, the lower the temperature is. This means that for a given Al content the solid solubility for Nb in ordered FeAl increases with decreasing temperature.

The general increase in the solid solubility of Nb in (αFe, Al) in dependence on temperature agrees with the normal behaviour expected for solid solutions. The behaviour in FeAl could be explained as follows: Thermodynamic calculations show a preferential site occupation of Nb within the B2 lattice of FeAl, on Fe sites, according to earlier calculations,[26] but more likely on Al sites,
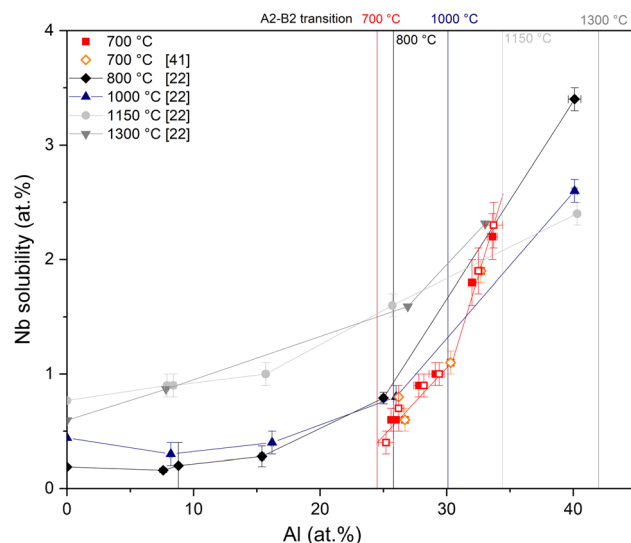
according to more recent ab-initio calculations.[42,43] If Nb has a site preference, it becomes likely that the solid solubility may increase with decreasing temperature, because long-range order increases with decreasing temperature. A possible explanation for the marked increase in the solid solubility of Nb in FeAl above an Al content of 30 at.% could be that a certain site occupation by Al has to be reached before a marked substitution by Nb becomes possible.

3.4 Lattice Constants

XRD analysis shows that the Fe-Al matrix is $D0_3$-ordered Fe_3Al at room temperature, because the transition from B2-ordered FeAl to $D0_3$-ordered Fe_3Al during cooling cannot be suppressed by quenching.[28] $Nb(Fe,Al)_2$ was identified in all samples as the hexagonal C14 Laves phase polytype. The lattice constants of the two phases are summarised in Table 2.

Figure 4 shows the lattice constant a of Fe-Al in dependence on the Al and Nb content. Compared to binary Fe-Al, the lattice constant increases in the present samples with increasing Al and Nb content in the ternary Fe-Al-Nb. As the lattice constant increases linearly with increasing Al and Nb, but no dependency on the Al content in the binary Fe-Al[30] in the investigated range of about 25–35 at.% Al was observed, the lattice constant can be estimated from the current data in dependence on the Nb content. Lattice constants of the boron-doped alloys fit with the values of the boron-free alloys, so it has been concluded that boron doping has no effect on the lattice constant.

As shown in Table 2, the lattice constants a and c for $Nb(Fe,Al)_2$ Laves phase increase with increasing Al and Nb content. No influence of boron doping could be observed. In previous research[44,45] on binary $NbFe_2$ Laves phase, the lattice parameters were found to increase with the increasing Nb content.

3.5 Transition Temperatures

By heating the equilibrated alloys up to 1200 °C, temperatures for the $D0_3$-B2 and B2-A2 transitions in Fe-Al were determined by DTA. Figure 5 shows the curves of the first heating. The determined critical temperatures are summarised in Table 3 and temperatures for binary compositions with the same Al content are given for comparison.[38]

Comparison of the temperatures established from the ternary alloys and those doped with boron, but otherwise comparably Al contents, shows that the boron doping has no marked influence on the transition temperatures (Table 3). The Curie temperature of Fe_3Al in the present alloys decreases only by 8 K, from 438 to 430 °C, when

Fig. 3 Nb solubility in the FeAl matrix in the temperature range 700–1300 °C in dependence on the Al content. Data at 800 to 1300 °C are taken from,[22] data for pure Fe from.[39] Vertical lines indicate the A2-B2 transitions at the indicated temperatures.[7] Additional data at 700 °C for boron-doped alloys are taken from[41] Boron doped alloys from this research are shown as open symbols

Table 2 Lattice constants of Fe₃Al and the Laves phase and c/a ratio as determined by XRD

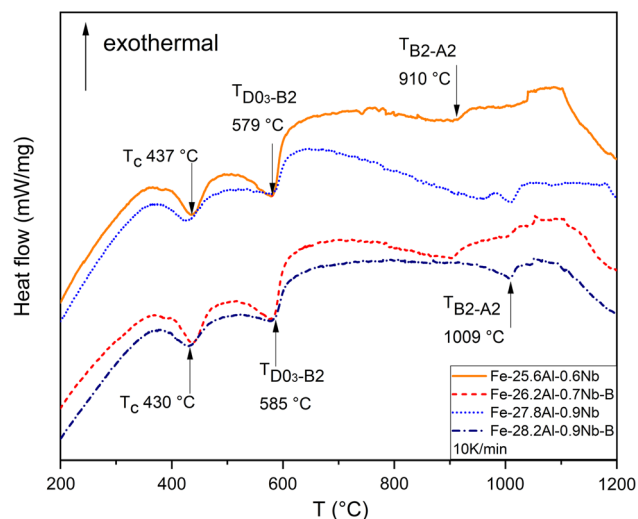| Alloy, at.%	Fe$_3$Al a, nm	Nb(Fe,Al)$_2$ a, nm	Nb(Fe,Al)$_{2,}$ c nm	Nb(Fe,Al)$_2$ c/a
Fe-24.4Al-2Nb-0.03B	0.57976(6)	0.4849(5)	0.792(2)	1.633
Fe-25.7Al-2Nb	0.57994(6)	0.4850(6)	0.7920(2)	1.633
Fe-25.7Al-2Nb-0.01B	0.57993(7)	0.485(2)	0.7919(7)	1.633
Fe-27.7Al-2Nb	0.58010(6)	0.4854(1)	0.793(4)	1.634
Fe-27.7Al-2Nb-0.01B	0.58016(7)	0.4851(2)	0.793(4)	1.635
Fe-27.7Al-3Nb	0.58019(5)	0.4862(6)	0.7931(2)	1.631
Fe-27.7Al-3Nb-0.01B	0.58035(1)	0.4867(6)	0.7932(2)	1.630
Fe-31.9Al-3Nb	0.58092(3)	0.488(2)	0.791(1)	1.623
Fe-31Al-3Nb-0.06B	0.58088(5)	0.4872(1)	0.795(2)	1.632
Fe-33.6Al-3Nb	0.58098(6)	0.487(4)	0.791(2)	1.624
Fe-33.6Al-3Nb-0.03B	0.58104(7)	0.4877(2)	0.794(6)	1.628
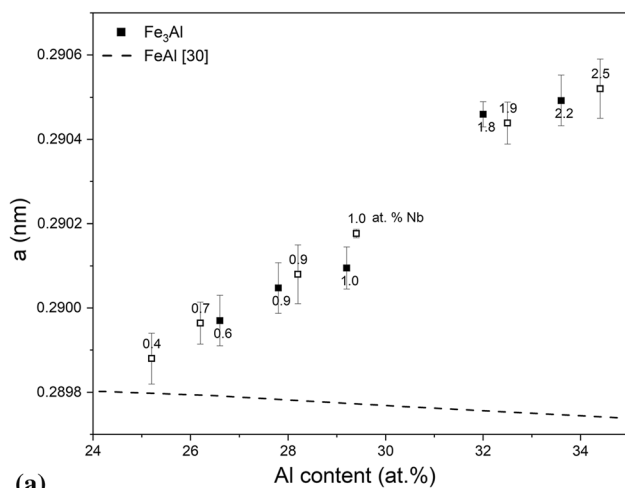
(a)
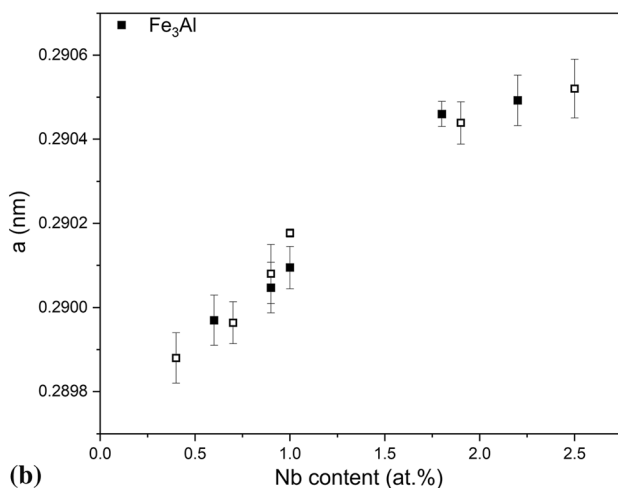
(b)

Fig. 4 Lattice constant of Fe-Al in dependence on the (a) Al and (b) Nb content. Values for Fe₃Al have been divided by 2. Symbols indicate the values obtained from the present Fe-Al-Nb(-B) samples and a dashed line for binary Fe-Al samples is shown for comparison.[30] Open symbols represent boron-doped alloys

Fig. 5 DTA heating cuves at 10 K/min

the D0₃-B2 transition temperatures increase by about 35 K compared to the binary alloys. Nb presumably substitutes Fe atoms at 4(b) sites in the D0₃ lattice, enhancing the atomic size mismatch effect (towards Al) and, therefore, the stability of D0₃.[24,46] As in the binary system the D0₃-B2 transition temperature does not change significantly within the, rather small, investigated range of Al contents. Compared to the binary system, the B2-A2 transition temperature increases by about 120 K by the addition of 2 at. % Nb. From 25.6 to 27.8 at.% Al, the B2-A2 transition temperature increases from 910 to 1009 °C in the ternary system. This correlates with the binary system where a comparable absolute increase of the B2-A2 transition temperature is observed for the same Al contents (Table 3).

No difference in the transition temperatures was observed for the two employed heating rates 10 and 20 K/min. This confirms that the observed temperatures stem from transitions without any diffusion, e.g. they are second order reactions, which is the case for the ferro- to

the Al content increases from 25.6 to 27.8 at.% Al, while in the binary system the Curie temperature drops by 110 K in Fe₃Al for the same Al contents. With the addition of Nb,

paramagnetic transition and the order/disorder transitions $D0_3$-B2 and B2-A2. It is noted, that the DTA investigations confirm that Fe-Al is B2-ordered FeAl at 700 °C, while the XRD patterns taken at room temperature showed $D0_3$-ordered Fe_3Al. This shows that also in the Fe-Al-Nb(-B) alloys this transition cannot be suppressed during cooling.

The solidus temperature of the boron-doped alloys are about 10 K lower than for the ternary alloys of comparable Al content. Comparison with the data of the binary system shows that for the same Al content the width of the solid–liquid interval increases from about 10 K to about 60 K by the addition of 2 at.% Nb (Table 4). However, it is known, that this difference will decrease with further increase in Nb and reaches 0 K at about 10 at.% Nb, along the eutectic valley.[22]

HT-XRD was carried out for the equilibrated alloy Fe-25.7Al-2Nb to confirm that the transformation temperatures observed by DTA are allocated to the correct phase transformations (Fig. 6). The $(111)_{D03}$ diffraction peak, which is the strongest superlattice diffraction peak of $D0_3$, disappears when heating from 560 to 600 °C, confirming that the transition temperature observed at 579 °C belongs to the $D0_3$-B2 transition. $(100)_{B2}$, the strongest superlattice diffraction peak of B2, disappears already when heating from 650 to 890 °C, though from DTA this transformation is only expected at 905 °C in this alloy. As already at 560 °C additional peaks of Fe_2O_3 are observed, the sample was oxidized, which presumably affects the B2-A2 transition temperature. For higher temperatures Fe_2O_3 transforms into Fe_3O_4 spinel plus γ-Al_2O_3. Formation of oxides

Table 3 Curie temperatures and transition temperatures of Fe-Al in the Fe-Al-Nb and boron-doped (*) alloys, heat treated 700 °C/1000 h. Data for binary Fe-Al for the same Al contents are shown for comparison[38]

Composition of Fe-Al, at.%	Fe-25.6Al-0.6Nb	Fe-26.2Al-0.7Nb*	Fe-27.8Al-0.9Nb	Fe-28.2Al-0.9Nb*	Fe-25.6Al [38]	Fe-27.8Al [38]
T_c (°C)	437	438	428	430	450	(340)
$T_{D03\leftrightarrow B2}$ (°C)	579	583	580	582	540	538
$T_{B2\leftrightarrow A2}$ (°C)	910	905	1009	1009	780	895

Table 4 Solidus and liquidus temperatures determined from as-cast Fe-Al-Nb(-B) alloys. Data for binary Fe-Al for the same Al content are shown for comparison[38]

Alloy composition, at.%	Fe-25.7Al-2Nb	Fe-25.7Al-2Nb-0.01B	Fe-27.7Al-2Nb	Fe-27.7Al-2Nb-0.01B	Fe-25.7Al [38]	Fe-27.7Al [38]
T_{sol} (°C)	1412	1402	1404	1395	1494	1481
T_{liq} (°C)	1470	1466	1450	1458	1505	1495

Fig.6 HT-XRD scans at different temperatures for Fe-25.7Al-2Nb, heat-treated 700 °C/1000 h

416

J. Phase Equilib. Diffus. (2022) 43:409–418
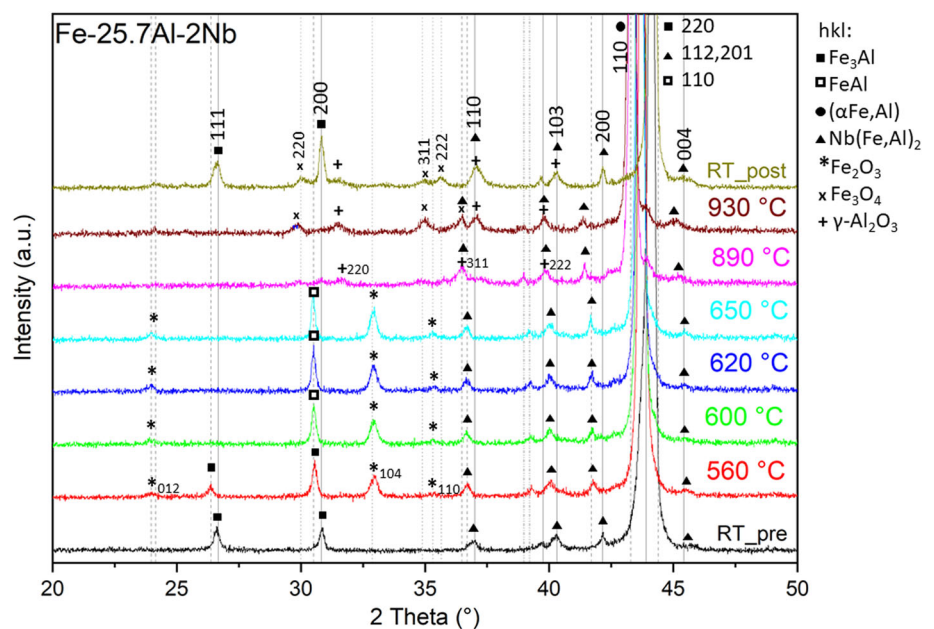
of Fe_2O_3, Fe_3O_4/$FeAl_2O_4$ spinel and metastable Al_2O_3 in iron aluminides at 700–900 °C was observed in[47] before. No further evaluation of the HT-XRD diffractogram has been undertaken in this study.

4 Conclusions

Phase equilibria between FeAl and $Nb(Fe,Al)_2$ have been determined at 700 °C between 24 and 34 at.% Al, a temperature and composition range of high interest for future alloy development. The results show that in Fe-Al-Nb(-B) alloys with Al contents between about 25 and 30 at.% Al, the solid solubility for Nb increases in FeAl from 0.5 to 1 at.% Nb, while the Nb content in $Nb(Fe,Al)_2$ increases from about 23 to 25.5 at.%. In alloys with Al contents between about 30 and 34 at.% Al the solid solubility for Nb in FeAl increases more markedly from 1.0 to 2.5 at.%, while the Nb content in $Nb(Fe,Al)_2$ stays constant at about 25 at.%. Though these changes may not appear to be large, they do have substantial implications for future alloy developments. Boron doping (maximum 0.06 at.%) was found not to affect the phase equilibria.

By changing the volume fraction of the Laves phase precipitates in the Fe-Al matrix, the mechanical properties can be adjusted, e.g. increasing the volume fraction will increase the strength of the alloy.[48,49] The present results show that for the same Nb content the volume fraction of $Nb(Fe,Al)_2$ precipitates will decrease with increasing Al content. The effect becomes more pronounced et al. contents above 30 at.% Al, where the solid solubility of Nb in FeAl increases markedly.

For a specific distribution of the Laves phase precipitates within the Fe-Al matrix the possibility of forming a metastable Fe_2XAl (X = Nb, Ta, Ti, Zr, Mo) Heusler phase prior to the formation of the stable Laves phase plays an important role.[35] Prerequisite for the formation of the Heusler phase is that the Fe-Al matrix becomes oversaturated in X during cooling. In that case the precipitation of metastable coherent Heusler phase precipitates is observed, which can be transformed to the stable Laves phase, e.g. through a heat treatment. Thereby the distribution of the Laves phase can be influenced, e.g. its precipitation preferentially at Fe-Al grain boundaries as coarse particles or fine-scaled and evenly distributed in the Fe-Al matrix.[35] Comparison of the solid solubility of Nb in Fe-Al at different temperatures (Fig. 3) reveals that only for compositions up to about 26 at.% Al, Fe-Al becomes oversaturated with Nb during cooling, while at higher Al contents the solid solubility increases with decreasing temperature. This explains why in a preceding study the metastable Heusler phase has only been observed in an alloy with about 25 at.% Al.[37]

Iron aluminide based alloys are well suited for casting parts.[3] The good casting properties of these materials are partly due to the small difference between liquidus and solidus temperatures, which helps to avoid residual coring during casting. In that sense, the increase of the liquid–solid interval from 10 K to about 60 K by the addition 2 at.% Nb (Table 4) is not favourable. However, no segregations have been observed in the Fe-Al matrix, which indicates that the observed increase should not be detrimental in view of casting respective alloys.

A very effective way of strengthening Fe-Al at higher temperatures is in stabilising the $D0_3$-order in respect to B2-order.[6] It has been known before that alloying with Nb can raise the $D0_3$-B2 transition temperature significantly,[24,25] though due to the limited solubility of Nb in Fe-Al in the studied composition range, it is not very effective which is again confirmed by the present DTA results (Table 4).

References

1. C.G. McKamey, Iron Aluminides, In: *Physical Metallurgy and Processing of Intermetallic Compounds*, 1996 N.S. Stoloff and V.K. Sikka, Editors, (Springer US Boston, MA, 1996), p. 351–391
2. D.G. Morris, and M.A. Muñoz-Morris, Recent Developments Toward the Application of Iron Aluminides in Fossil Fuel Technologies, *Adv. Eng. Mater.*, 2011, **13**, p 43–47.
3. M. Palm, F. Stein, and G. Dehm, Iron Aluminides, *Annu. Rev. Mater. Res.*, 2019, **49**(1), p 297–326. https://doi.org/10.1146/annurev-matsci-070218-125911
4. D. Hardwick, and G. Wallwork, Iron-Aluminium Base Alloys a Review of Their Feasibility as High Temperature Materials, *Rev. High-Temp. Mater.*, 1978, **4**, p 47–74.

5. D.G. Morris, Possibilities for High-Temperature Strengthening in Iron Aluminides, *Intermetallics*, 1998, **6**, p 753–758.

6. M. Palm, Concepts Derived from Phase Diagram Studies for the Strengthening of Fe-Al-Based Alloys, *Intermetallics*, 2005, **13**, p 1286–1295.

7. A. Malfliet, F. Stein, T. Vaubois, and K.C.H. Kumar, Al-Fe-Nb Ternary Phase Diagram Evaluation, in *MSI Eureka*. G. Effenberg, Ed., Materials Science International, Stuttgart, 2017, p 1–40

8. D.G. Morris, M.A. Muñoz-Morris, and C. Baudin, The High-Temperature Strength of Some Fe₃Al Alloys, *Acta Mater.*, 2004, **52**, p 2827–2836.

9. N. Matsumoto, Y. Kaneno, and T. Takasugi, Strengthening and Ductilization of D0₃-Type Fe₃Al Intermetallic Alloys by Dispersion of Laves Phases Fe₂Zr and Fe₂Nb, *Mater. Sci. Forum*, 2007, **561–565**, p 395–398.

10. S.A. Azmi, A. Michalcová, L. Senčeková, and M. Palm, Microstructure and Mechanical Properties of Fe–Al–Nb–B Alloys, *MRS Adv.*, 2017, **2**, p 1353–1359.

11. P. Kratochvíl, M. Švec, R. Král, J. Veselý, P. Lukáč, and T. Vlasák, The Effect of Nb Addition on the Microstructure and the High-Temperature Strength of Fe3Al Aluminide, *Metall. Mater. Trans. A.*, 2018, **49**, p 1598–1603.

12 F. Dobeš, P. Dymáček, and M. Friák, The Influence of Niobium Additions on Creep Resistance of Fe-27 at. % Al Alloys, *Metals*, 2019, **9**(7), p 739. https://doi.org/10.3390/met9070739

13. D.M. Dimiduk, M.G. Mendiratta, D. Banerjee, and H.A. Lipsitt, A Structural Study of Ordered Precipitates in an Ordered Matrix Within the Fe-Al-Nb System, *Acta Metall.*, 1988, **36**, p 2947–2958.

14. D.G. Morris, L.M. Requejo, and M.A. Muñoz-Morris, A Study of Precipitation in D0₃ Ordered Fe-Al-Nb Alloy, *Intermetallics*, 2005, **13**, p 862–871.

15. C. Guo, T. Wu, C. Li, and Z. Du, Thermodynamic Description of the Al-Fe-Nb System, *Calphad*, 2017, **57**, p 78–87.

16. C. He, Y. Qin, and F. Stein, Thermodynamic Assessment of the Fe-Al-Nb System with Updated Fe-Nb Description, *J. Phase Equilib. Diffus.*, 2017, **38**, p 771–787.

17. A.A.A.P. Da Silva, *Thermodynamic Modeling and Critical Experiments on the Al-Fe-Nb System,* PhD thesis, Escola de Engenharia de Lorena, Universidade de Sao Paulo, Brazil 2015, p. 1–168.

18. V.V. Burnashova, V.R. Ryabov, and V.Y. Markiv, Investigation of Nb-Fe-Al and Nb-Co-Al Systems, *Dop Akad Nauk Ukr RSR/A*, 1970, **1970**, p 747–750.

19. M. Palm, Phase Equilibria in the Fe Corner of the Fe-Al-Nb System Between 800 and 1150 °C, *J. Alloys Compd.*, 2009, **475**, p 173–177.

20. J.M. Zelaya Bejarano, *Estudo do Diagrama Ternário Ferro-Alumínio-Nióbio,* Estudo do Diagrama Ternário Ferro-Alumínio-Nióbio, PhD thesis, Universidade Estadual de Campinas, Brazil, 1993, p. 1–148.

21. F. Stein, C. He, O. Prymak, S. Voß, and I. Wossack, Phase Equilibria in the Fe-Al-Nb System: Solidification Behaviour, Liquidus Surface and Isothermal Sections, *Intermetallics*, 2015, **59**, p 43–58.

22. O. Prymak, and F. Stein, Solidification and High-Temperature Phase Equilibria in the Fe-Al-Rich Part of the Fe-Al-Nb System, *Intermetallics*, 2010, **18**, p 1322–1326.

23. L.T.F. Eleno, L.A. Errico, P.G. Gonzales-Ormeño, H.M. Petrilli, and C.G. Schön, Ordering Phase Relationships in Ternary Iron Aluminides, *Calphad*, 2014, **44**, p 70–80.

24. L. Anthony, and B. Fultz, Effects of Early Transition Metal Solutes on the D0₃–B2 Critical Temperature of Fe₃Al, *Acta Metall. Mater.*, 1995, **43**, p 3885–3891.

25. F. Stein, A. Schneider, and G. Frommeyer, Flow Stress Anomaly and Order-Disorder Transitions in Fe₃Al-Based Fe-Al-Ti-X Alloys with X=V, Cr, Nb, or Mo, *Intermetallics*, 2003, **11**, p 71–82.

26. A.O. Mekhrabov, and M.V. Akdeniz, Effect of Ternary Alloying Elements Addition on Atomic Ordering Characteristics of Fe-Al Intermetallics, *Acta Mater.*, 1999, **47**, p 2067–2075.

27. A. Bradley, and A. Jay, The Lattice Spacings of Iron-Aluminium Alloys, *J. Iron Steel Inst. London*, 1932, **125**, p 339–357.

28. A. Taylor, and R.M. Jones, Constitution and Magnetic Properties of Iron-Rich Iron-Aluminium Alloys, *J. Phys. Chem. Solids*, 1958, **6**, p 16–37.

29. H. Okamoto, and P.A. Beck, Phase Relationships in the Iron Rich Fe-Al Alloys, Metallurgical, *Transactions*, 1971, **2**, p 569–574.

30. U.R. Kattner, and B.P. Burton, Al-Fe, in *Phase Diagrams of Binary Iron Alloys*. H. Okamoto, Ed., ASM International, Materials Park (OH), 1993, p 12–28

31. M. Palm, Fe-Al Materials for Structural Applications at High Temperatures: Current Research at MPIE, *Int. J. Mater. Res.*, 2009, **100**, p 277–287.

32. C. J. Smithells, and E. A. Brandes, *Smithells Metals Reference Book* ed. E.A. Brandes and G.E. Brook. Vol. 7, (Oxford Butterworth, Heinemann, 1992)

33. D.D. Risanti, and G. Sauthoff, Microstructures and Mechanical Properties of Fe-Al-Ta Alloys with Strengthening Laves Phase, *Intermetallics*, 2011, **19**, p 1727–1736.

34. D.G. Morris, M.A. Munoz-Morris, and L.M. Requejo, New iron-Aluminium Alloy with Thermally Stable Coherent Intermetallic Nanoprecipitates for Enhanced High-Temperature Creep Strength, *Acta Mater.*, 2006, **54**, p 2335–2341.

35. P. Prokopčáková, M. Švec, and M. Palm, Microstructural Evolution and Creep of Fe-Al-Ta Alloys, *Int. J. Mater. Res.*, 2016, **107**, p 396–405.

36. A.A. Coelho, TOPAS and TOPAS-Academic: Ann Optimization Program Integrating Computer Algebra and Crystallgraphic Objects Written in C++, *J Appl Crystallogr*, 2018, **51**, p 210–218.

37. A. Gedsun, F. Stein, and M. Palm, Development of New Fe-Al-Nb(-B) Alloys for Structural Applications at High Temperatures, *MRS Adv.*, 2021, **6**, p 176–182.

38. F. Stein, and M. Palm, Re-Determination of Transition Temperatures in the Fe-Al System by Differential Thermal Analysis, *Int. J. Mater. Res.*, 2007, **98**, p 580–588.

39. E. Paul, and L.J. Schwartzendruber, The Fe-Nb System, *Bull. Alloy Phase Diagr.*, 1986, **7**, p 248–254.

40. F. Stein, G. Sauthoff, and M. Palm, Phases and Phase Equilibria in the Fe-Al-Zr System, *Z. Metallkd.*, 2004, **95**, p 469–485.

41. S.A. Azmi, . *Microstructures and Mechanical Properties of Iron Aluminide-Based Fe-Al-Nb-B Alloys,* Master thesis, RWTH Aachen, Germany, 2015

42. G.H. Bozzolo, R.D. Noebe, and C. Amador, Site Occupancy of Ternary Additions to B2 Alloys, *Intermetallics*, 2002, **10**, p 149–159.

43. Y. Zheng, F. Wang, T. Ai, and C. Li, Structural, Elastic and Electronic Properties of B2-type Modified by Ternary Additions FeAl-Based Intermetallics: First-Principles Study, *J. Alloy. Compd.*, 2017, **710**, p 581–588.

44. D. Grüner, *Untersuchungen zur Natur der Laves-Phasen in Systemen der Übergangsmetalle,* PhD thesis, TU Dresden, Germany, online available at http://nbn-resolving.de/urn:nbn:de:swb:14-1172078219643-48967, (2007), p. 1–276.

45. S. Voß, *Mechanische Eigenschaften von Laves Phasen in Abhängigkeit von Kristallstruktur und Zusammensetzung am Beispiel der Systeme Fe-Nb(-Al) und Co-Nb (Mechanical Properties of Laves Phases in Dependence on Crystal Structure and Composition Using the Example of the Systems Fe-Nb(-Al) and Co-Nb*, Ph.D. thesis, RWTH Aachen: Shaker Verlag, Aachen, 2012, p. 1–131.

418

J. Phase Equilib. Diffus. (2022) 43:409–418

46. G. Frommeyer, C. Derder, and J.A. Jimenez, Superplasticity of Fe$_3$Al(Cr), *Mater. Sci. Technol.*, 2002, **18**, p 981–986.

47. B. Pöter, F. Stein, R. Wirth, and M. Spiegel, Early Stages of Protective Oxide Layer Growth on Binary Iron Aluminides, *Z. Phys. Chem.*, 2005, **219**, p 1489–1503.

48. F. Stein, M. Palm, and G. Sauthoff, Mechanical Properties and Oxidation Behaviour of Two-Phase Iron Aluminium Alloys with Zr(Fe, Al)$_2$ Laves Phase or Zr(Fe, Al) τ_1 1 Phase, *Intermetallics*, 2005, **13**, p 1275–1285.

49. S. Milenkovic, and M. Palm, Microstructure and Mechanical Properties of Directionally Solidified Fe-Al-Nb eutectic, *Intermetallics*, 2008, **16**, p 1212–1218.

Publisher's Note Springer Nature remains neutral with regard to jurisdictional claims in published maps and institutional affiliations.